Eur. Phys. J. B **58**, 223–230 (2007)
DOI: 10.1140/epjb/e2007-00225-1

THE EUROPEAN PHYSICAL JOURNAL B

Modelling of dynamical processes in a molecular crystal by NMR

R. Decressain[1,a], L. Carpentier[1], E. Cochin[1], and J.P. Amoureux[2]

[1] LDSMM, CNRS UMR 8024, Université de Lille-1, 59655 Villeneuve d'Ascq, France
[2] LCPS, Université de Lille-1, 59655 Villeneuve d'Ascq, France

Received 16 November 2006 / Received in final form 20 June 2006
Published online 8 September 2007 –

Abstract. In this contribution we report on the plastic crystal 1-chloroadamantane dynamics via conventional frequency dependent (^{1}H and ^{13}C) and field cycling NMR measurements. A suitable microscopic dynamical model, worked out from from X-ray analysis is developed and the molecular motions are interpreted in terms of: self diffusion and dipolar molecular axis combined with uniaxial rotation. In the rotator phase the molecules execute a bimodal reorientation process whereas the uniaxial rotation solely persists in the low temperature phase. In both phases, the residence times exhibit an Arrhenius temperature dependence. The results confirm the existence of a dynamic crossover transition predicted by molecular dynamics simulation.

PACS. 76.60.-k Nuclear magnetic resonance and relaxation – 61.50.-f Crystalline state – 76.60.Es Relaxation effects

1 Introduction

Molecular crystals made of globular molecules often exhibit an orientationnally disordered or rotator phase commonly called plastic phase (PC) according to the original definition of Timmermans [1]. For many years plastic crystals have been studied, and particular attention was focused on their polymorphism, structural and dynamical properties [2–13]. Upon cooling, when the orientationnal ordering is avoided, some plastic crystals can freeze into a glassy state [2–4]. Well-known examples are carboranes, cyclo-hexanol, ethanol and Cyano-Adamantane ($C_{10}H_{15}CN$:CN-ADM) [4]. The supercooled plastic crystalline phase presents, as for glass forming liquids, dynamic and thermodynamic manifestations of a glass transition: the main relaxation (α process) is non-Arrhenius and a steplike change in the heat capacity is observed at the calorimetric glass transition. As a consequence, since they involve only orientational degrees of freedom, glassy crystals are considered as model systems for glass transition investigations. Although most of the monosubstituted adamantanes ($C_{10}H_{16}$: ADM) exhibit a rotator phase, CN-ADM is, to our knowledge, the only example giving rise to a glassy state. This peculiarity has motivated numerous studies on this compound during the last years [5–10]. From a dynamic point of view, the CN substituent leads to an important activation energy of the dipolar axis motion (α process) directly involved in the glass transition mechanism.

The main purpose of this work was to investigate the dynamics of 1-chlorodamantane ($C_{10}H_{15}$Cl:CL-ADM). This compound presents an orientationally disordered phase (PC: phase I) of space group Fm3m [11]. CL-ADM undergoes a solid-solid phase transition at T_t = 244.2 K (24.61 JK^{-1} mol^{-1}) and melts at T_m = 442.5 K (11.01 JK^{-1} mol^{-1}) [13]. The low temperature phase (phase II) is orientationally ordered (monoclinic) of space group $P_{21/c}$ [12]. Molecular dynamic (MD) simulations have revealed that some features of CL-ADM were consistent with the mode coupling theory (MCT) [14]. A crossover between two dynamical regimes at T_x = 330 K, interpreted as a change in the energy landscape topography was reported [9,15]. The precise nature of this temperature, found above the critical temperature T_c corresponding to an ergodic-nonergodic transition, remains unclear. Experimental extensions are needed to validate the MCT picture. In CL-ADM, a wide frequency range investigation of the dynamics, particularly above T_x, is missing and has motivated the present study by ^{1}H and ^{13}C NMR. NMR is one of the most powerful method for dynamics investigations by means of relaxation rates measurements. An alternative technique, Field Cycling NMR (FCNMR), allowing low frequencies relaxation times measurements over several decades was recently developed and applied in various systems with complex dynamics [16]. This technique measure the spectral densities from T_{1z} (ν) and is consequently very efficient to detect multi modal processes or dynamical heterogeneities. In plastic crystals, the experimental data can be analysis by a Frenkel model, originally developed by Virlet, Quiroga and Amoureux [17].

[a] e-mail: regis.decressain@univ-lille1.fr

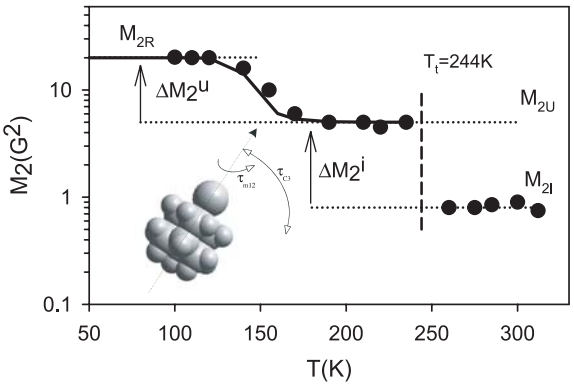

Fig. 1. Second moment M_2 of the proton NMR line versus temperature. Dotted lines represent the calculated second moment for: rigid lattice (M_{2R}), uniaxial rotation (M_{2U}) and isotropic rotation (M_{2I}). Inset: schematic representation of a $C_{10}H_{15}Cl$ molecule with the uniaxial rotation (τ_{m12}) and the tumbling motion (τ_{c3}). Below T_t, where only uniaxial rotation persists, the solid line is calculated by equation (19), using the motional parameters τ_{m3} given in Table 2.

The reliability of this model, based on the description of a master equation using the group theory, has already been demonstrated on Bicyclo-octane and some ADM derivatives [18–20]. This formalism is presently applied to CL-ADM.

The paper is organised as follows. The next section presents the experimental details relevant to this study. A description of the Frenkel model is given in Section 3. The NMR results are presented and compared with those obtained with other techniques in Section 4.

2 Experimental

CL-ADM was synthesized in our laboratory from ADM ($C_{10}H_{16}$) by replacing one methine hydrogen by a chlorine atom (inset of Fig. 1). High fields NMR experiments were performed on Bruker wide-bore ASX spectrometers. ^{13}C measurements were carried out at 25 and 100 MHz using simultaneously Magic Angle Spinning (MAS) at 3 KHz and ^1H decoupling (100 W) during acquisition. ^1H experiments were performed at 100, 200, and 400 MHz. Low field NMR experiments were performed on a home build spectrometer operating at 48 MHz. The proton second moments M_2 were obtained by a signal integration from a C.W. VARIAN spectrometer operating at 15 MHz. The proton spin-spin relaxation times T_2 were measured with a pulse-echo sequence at 100 MHz, T_{1z} values with the magnetisation recovery pulse sequence $(\pi,\ \tau,\ \pi/2,\ D_0)_n$, with typically 16τ values and a recycle delay $D_0 > 5T_{1z}$. The rotating frame spin-lattice relaxation time $T_{1\rho}$ was determined by locking the signal after a $\pi/2$ pulse with a $\pi/2$ phase-shifted pulse and then observing the signal intensity as a function of the spin-locking pulse duration. A 18 G field pulse (H_1) was employed. The sample temperature was varied from T_m to 120 K with an accuracy of ± 1 K with either precooled nitrogen or preheated air gas flows. The experiments were carried out on powder samples in glass tubes sealed under vacuum. The reproducibility of the results was checked by recording the spectra during cooling and heating cycles, in all cases the magnetisation recoveries were found exponential. In the high temperature range, T_{1D} measurements were performed at 100 MHz by using the Jeener-Broekaert pulse sequence [21]:

$$\left[(\frac{\pi}{2})_{0^\circ} - t - (\frac{\pi}{4})_{90^\circ} - \tau - (\frac{\pi}{4})_{90^\circ}\right].$$

The accuracy of the NMR data obtained under such experimental conditions lies between 5% for T_1 and 15% for M_2.

Field Cycling NMR (FCNMR) measurements were carried out with a Stelar Spinmaster FFC 2000 relaxometer (Stelar, Pv, Italy). The nuclear magnetic relaxation dispersion profiles $T_{1z}(\nu)$ were measured from 0.1 to 15 MHz at 301, 333 and 353 K.

3 Models for NMR analysis

The general theory of magnetic dipole-dipole nuclear spin relaxation has been treated in many standard books [22,23]. Assuming a dipolar interaction mechanism, the proton spin-lattice relaxation time is given by:

$$\frac{1}{T_{1z}} = \sum_i C_i \left[J(\omega, \tau_i) + 4J(2\omega, \tau_i)\right] \qquad (1)$$

where C_i is the dipolar constant, ω is the Larmor frequency and $J(\omega, \tau_i)$ is the spectral density function defined as the Fourier transform of an autocorrelation function $G(t)$.

When the motion is considered as isotropic, the correlation function corresponds to a single exponential ($G(t) \propto e^{-t/\tau}$) and the spectral density turns out to be Lorentzian (BPP model [24]):

$$J(\omega, \tau) = L(\omega, \tau) = \frac{\tau}{1 + \omega^2\tau^2}. \qquad (2)$$

For plastic crystals, the existence of a crystal lattice imposes a limited number of molecular equilibrium positions. This Frenkel model, already described in references [19,20], is based on the following hypothesis:

- all successive orientations are deduced from each other by the symmetry operations of a rotational group,
- the jump times are negligible with respect to the residence times,
- two successive reorientations are completely uncorrelated,
- the probability for a particular reorientation to occur is identical for all operations of the group belonging to the same class (central force hypothesis).

In ADM, assuming molecular reorientations around fixed (crystallographic) and mobile (molecular) axis, the correlation functions for the O $\otimes$ C_n group are given for a

Table 1. τ_α correlation times and $\varphi_\alpha$coefficients for CL-ADM versus α according to references [19,20].

α	1	2	3	4	5	6
$\frac{1}{\tau_\alpha}$	$\frac{1}{\tau_T}$	$\frac{1}{\tau_T}+\frac{1}{\tau_{r1}}$	$\frac{1}{\tau_T}+\frac{1}{\tau_{r2}}$	$\frac{1}{\tau_E}$	$\frac{1}{\tau_E}+\frac{1}{\tau_{r1}}$	$\frac{1}{\tau_E}+\frac{1}{\tau_{r2}}$
$\varphi_\alpha^{\mathrm{H}}$	0	0.339	0.206	0.249	0	0.206
$\varphi_\alpha^{C\mathfrak{x}}$	0	0.069	0.349	0.233	0	0.349
$\varphi_\alpha^{C\mathfrak{y}}$	0	0.256	0.305	0.134	0	0.305
$\varphi_\alpha^{C\mathfrak{z}}$	0	0.306	0.284	0.126	0	0.284
φ_α^{C4}	0	0.177	0.141	0.541	0	0.141

powder sample by:

$$G(t) = \sum_{\alpha=1}^{6} \varphi_\alpha e^{-\frac{t}{\tau_\alpha}}. \tag{3}$$

The equilibrium positions and the molecular geometry are taken into account by the φ_α terms as defined in Table 1a of reference [19]. For ADM derivatives, we have derived the ^{1}H and ^{13}C relaxation rates expressions:

$$\frac{1}{T_{1z}^H} = \frac{2}{3} M_2(\mathrm{H}) \sum_{\alpha=1}^{6} \varphi_\alpha^H \left[L(\omega_H,\tau_\alpha) + 4L(2\omega_H,\tau_\alpha)\right] = \frac{2}{3} M_2(H) \sum_{\alpha=1}^{6} \Psi_\alpha^H \tag{4}$$

$$\frac{1}{T_{1\rho}^H} = \frac{2}{3} M_2(\mathrm{H}) \sum_{\alpha=1}^{6} \varphi_\alpha^{\mathrm{H}} \left[\frac{3}{2} L(2\omega_1,\tau_\alpha) + \frac{5}{2} L(\omega_H,\tau_\alpha) + L(2\omega_H,\tau_\alpha)\right] \tag{5}$$

$$\frac{1}{T_{1z}^C} = \frac{2}{3} M_2(\mathrm{C}) \sum_{\alpha=1}^{6} \varphi_\alpha^C \left[\frac{1}{3} L(\omega_C-\omega_H,\tau_\alpha) + L(\omega_C,\tau_\alpha) + 2L(\omega_C+\omega_H,\tau_\alpha)\right] = \frac{2}{3} M_2(\mathrm{C}) \sum_{\alpha=1}^{6} \Psi_\alpha^C \tag{6}$$

with: $\omega_i = \gamma_i\ B_0$ ($i =^1$H or ^{13}C); $\omega_1 = \gamma_H B_1$.

The second moments are given by the relations [22]:

$$M_2(\mathrm{H}) = \frac{9}{20} \hbar^2 \gamma_H^4 \sum_{k\neq 1} r_{k1}^{-6} \tag{7}$$

$$M_2(\mathrm{C}_m) = \frac{9}{20} \hbar^2 \gamma_C^2 \gamma_H^2 \sum_{k} r_{km}^{-6}. \tag{8}$$

The (k,l,m) indices describe the protons and carbons in the molecule, the other symbols have their general meaning [23].

For the symmetry group (O $\otimes$ C$_n$), we have obtained [17–20,25]:

$$\frac{1}{\tau_E} = \frac{1}{\tau_{C4}} + \frac{1}{\tau_{C2'}} + \frac{3}{2\tau_{C3}} \tag{9}$$

$$\frac{1}{\tau_T} = \frac{4}{3\tau_{C4}} + \frac{2}{3\tau_{C2'}} + \frac{1}{\tau_{C3}} + \frac{4}{3\tau_{C2}}. \tag{10}$$

The residence time $\tau_{c\beta}$ (β = 2, 2', 3, 4; c = cubic) represents the mean time an intra-molecular inter-nuclei vector $\mathbf{r}$ spends before turning around any of the cubic axes belonging to the β class of the O group. The τ_{mp} residence time represents the mean time this vector spends before rotating by $\pm 2\pi/p$ around the molecular axis. The decomposition of τ_{rq} ($q = 1, 2$) versus τ_{mp} is given by [17–20,25]:

$$\frac{1}{\tau_{rq}} = 2 \sum_{p}^{n} \frac{\sin^2\left(\pi \frac{q}{p}\right)}{\tau_{mp}} \tag{11}$$

where p is an integer dividing the order of the rotational group. The τ_α decomposition is given in Table 1. The BPP model (Eq. (1)), can be deduced from relations (4–6) by taking: $\tau_\alpha = \tau$ ($\forall\alpha$).

In the following the correlation times τ are assumed to follow an Arrhenius law:

$$\tau(s) = \tau_0\ e^{\frac{E}{T}} \tag{12}$$

where E(K) the activation energy and τ_0(s) the pre-exponential factor are characteristic parameters of the motion.

3.1 Analysis of ^{1}H data

In solids, molecular motions average the local field causing line narrowing when frequencies exceed the NMR spectral line width. In adamantanes the ^{1}H NMR line is mainly determined by dipolar interactions and the second moment can be calculated (Eqs. (7,8); [22]). From the experimental CL-ADM second moment (M_2; Fig. 1) and FID (T_2; Fig. 2) the following properties were established. In phase I, the experimental $M_2 \approx 0.75G^2$ is characteristic of fast isotropic reorientations (Isotropic: $M_{2I} = 0.6G^2$); [26]). Between 244 K and 150 K (phase II), the plateau of $M_2 \approx 5G^2$ corresponds to uniaxial rotation around the threefold (C3) axis (Uniaxial: $M_{2u} = 5.4G^2$; [26]). Below 150 K, the line broadens and a rigid lattice value is reached $M_2 \approx 21G^2$ (Rigid: $M_{2R} = 23G^2$; [26]). At temperatures above $T \approx 330$ K an additional line narrowing occurs, the resonance line shape becomes Lorentzian and M_2 is no longer defined.

The ^{1}H relaxation times are represented in Figure 2, versus reciprocal temperature. The $T_{1\rho}$ measurements are performed in phase (II) and in the high temperature range of phase (I), whereas T_{1z} extends from 130 K up to the vicinity of T_m. The dipolar relaxation time T_{1D}, which gives a description of very slow molecular motions, is only measured in the plastic phase (I). To avoid effects due to

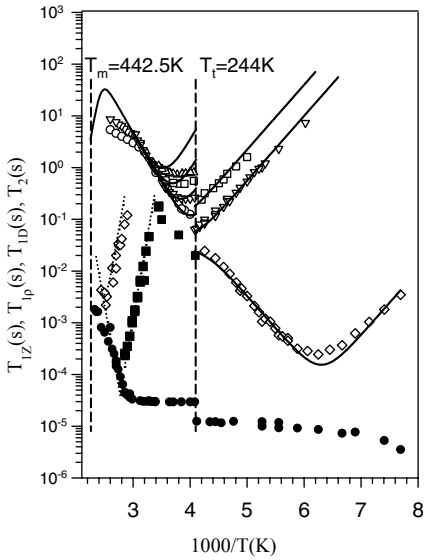

Fig. 2. Variation of ^{1}H NMR relaxation times versus $10^3/T$(K): T_{1z} (◯) 48 MHz, (▽) 100 MHz, (□) 200 MHz, (△) 400 MHz; $T_{1\rho}$ (◊); T_{1D} (■); T_2 (●). The dotted lines ($T_{1\rho}$; T_{1D}) describe the self diffusion mechanism fitted with equations (14, 15). In phase I, the continuous curves represent the best simultaneous fit obtained with a B.P.P. model and a SD contribution (Eq. (17)). The corresponding parameters are given in Tables 2 and 3.

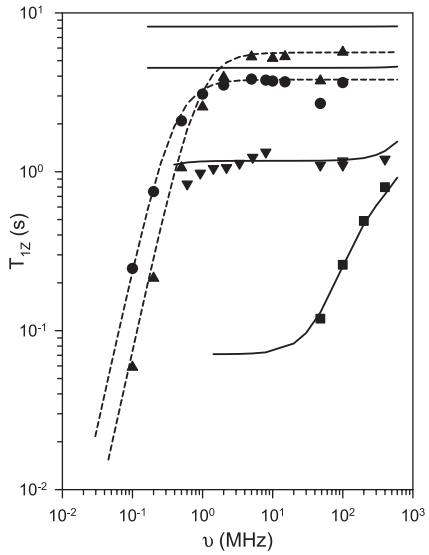

Fig. 3. ^{1}H FCNMR profiles taken at three temperatures in the plastic phase: (■) 250 K, (▼) 301 K, (●) 333 K, (▲) 353 K. The dashed lines represent the best fit to the experimental data using equation (17). The solid curves represent T_{1z} calculated by assuming a Frenkel model (Eq. (4); Tab. 2).

phase transformation kinetics near T_t, the values in the ordered phase are obtained after a long isotherm. Under such conditions, both T_{1z} and T_2 exhibit discontinuities at T_t. In phase (I) below T_x, from the second moment analysis, fast motions are monitored by the Zeeman relaxation. Under the extreme narrowing limit, a motional activation energy is obtained: $E_a = 4300$ K. A change of E_a (4300 K to 1400 K) is observed around T_x. The FCNMR profiles (Fig. 3; $T = 301$, 333, 353 K) suggest the existence of two relaxation modes in phase (I). At high frequency, as expected under a fast motion regime, T_{1z} is constant. At low frequency the T_{1z} drop indicates the occurrence of a new relaxation process. This drop shifts to higher frequencies as the temperature increases thus reflecting a thermally activated process.

3.1.1 Plastic phase

A quantitative analysis of the experimental data was performed by assuming an isotropic molecular reorientation (BPP model; [24]). An attempt to match all together the experimental data ($T < 400$ K) using equation (1) is represented in Figure 2. The corresponding parameters are given as τ_{BPP} in Table 2. At high temperature and below T_x this model gives a good description of the data for the low magnetic fields. For higher fields, discrepancies are clearly observed below the T_{1z} minima.

A different procedure for the interpretation of the data consists to construct a master curve from measurements taken at different Larmor frequencies [27]. This model free approach has proven to be efficient in polymers analysis, even if the details of global motions cannot be obtained [19,28]. In Figure 4a, we have plotted $\log(\omega_0/T_1(T))$ versus $\log(\omega_0\tau_c(T))$, where $\tau_c(T)$ is the relevant correlation time. As seen in Figure 4a, several relaxation modes contribution in the T_{1z} NMR time window (10^{-8}–10^{-12}s) are observed. As a consequence an interpretation based on a single correlation time may be misleading.

We have then considered a Frenkel model assuming $\pi/6$ rotations around the molecular C_3 axis (τ_{m12}) and the tumbling of this axis along the [100] lattice directions (τ_{c3}) (Eqs. (4,5 [29,30])). The curves corresponding to the best refinement (Tab. 2) are represented as solid lines in Figures (3 and 5). Below T_x, this model allows an accurate description of the experimental data for every studied

Table 2. Dynamical parameters obtained by different techniques for CL-ADM. The NMR parameters were obtained by using a model assuming: (a) isotropic rotational diffusion, (b) uniaxial rotation, (c) reorientations around molecular axis together with uniaxial rotation.

Phase	τ_i	τ_0 (s)	E_a (K)	Technics
Plastic	τ_{BPP}	0.44×10^{-16}	4400	RMN $^{(a)}$
	τ_{C3}	0.76×10^{-16}	4360	^{1}H, ^{13}C RMN $^{(c)}$
	//	2.6×10^{-15}	3370	Dielectric [33]
	//	10.9×10^{-15}	2574	I.Q.N.S. [29]
	τ_{m12}	0.19×10^{-15}	2840	^{1}H RMN $^{(c)}$
	//	0.51×10^{-12}	1330	^{13}C RMN $^{(c)}$
	//	12.3×10^{-15}	1240	I.Q.N.S. [29]
Ordered	τ_{BPP}	0.13×10^{-13}	2890	^{1}H RMN $^{(a)}$
	τ_{m3}	0.33×10^{-14}	2860	^{1}H, ^{13}C RMN $^{(b)}$

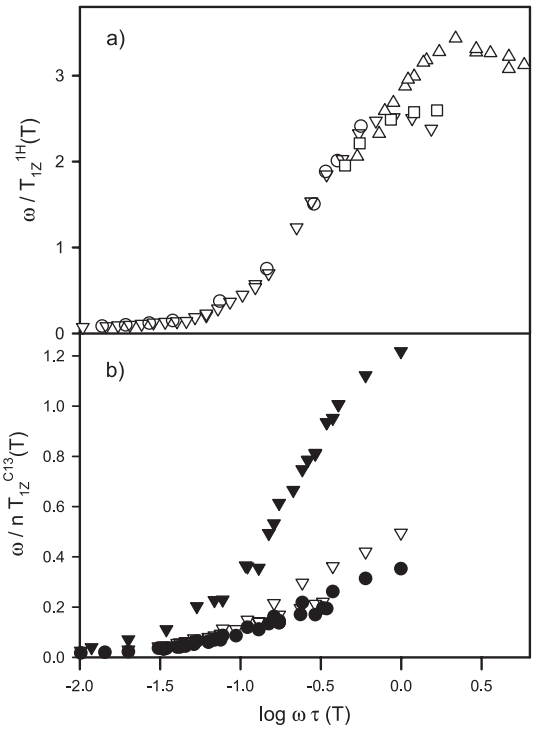

Fig. 4. Superposition of relaxation rates as a function of the reduced variable $\omega_0\tau(T)$: (a) ^{1}H at (◯) 48 MHz, (▽) 100 MHz, (□) 200 MHz, (△) 400 MHz and (b) ^{13}C at 25 and 50 MHz, (●) C_2, (▽) C_3, (▼) C_4

magnetic fields. Nevertheless, the experimental data above T_x are not correctly reproduced.

In plastic crystals translational self diffusion (SD: τ_{SD}) is known to give a significant relaxation mechanism, near the melting point [2]. For a quantative analysis we have used the Torrey's isotropic random-walk model for self diffusion on a face centered cubic (f.c.c.) lattice [2]:

$$(\omega_0\tau_{SD} \ll 1)\text{: } \frac{1}{T_2} = \frac{1}{T_{1\rho}} = 0.922 M_2 \tau_{SD} \qquad (13)$$

$$(\omega_0\tau_{SD} \gg 1)\text{: } \frac{1}{T_{1\rho}} = 0.429 \frac{M_2}{\omega_1^2 \tau_{SD}}. \qquad (14)$$

Below the temperature of the T_{1D} minimum and under the conditions $\tau_{SD} \gg T_2$ and $\omega_0\tau_{SD} \gg 1$, we have [2]:

$$\frac{1}{T_{1D}} = \frac{2(1-p)}{\tau_{SD}}. \qquad (15)$$

For a f.c.c. lattice, $p = 0.2234$ [2]. Using equations (13–15), as seen in Figure 2, the experimental results are well described by using the parameters of Table 3. The activation energy is consistent with other adamantanes derivatives [2,10]. When approaching T_m, due to a sublimation effect, the experimental T_2 are somewhat smaller than those predicted by equation (13). Using these parameters, we tried to describe the data above T_x. The SD contribution to T_{1z} is given by [2]:

$$\frac{1}{T_{1z}} = 2.29 \frac{M_2}{\omega_0^2 \tau_{SD}}. \qquad (16)$$

Table 3. Translational diffusion parameters obtained for CL-ADM and ADM.

Compounds	τ_0 (s)	E_a (K)	Technics
CL-ADM	2×10^{-22}	14570	NMR (this work)
ADM	1.6×10^{-21}	18450	NMR [2,30]
	4.6×10^{-20}	16646	Radio Tracer [2]

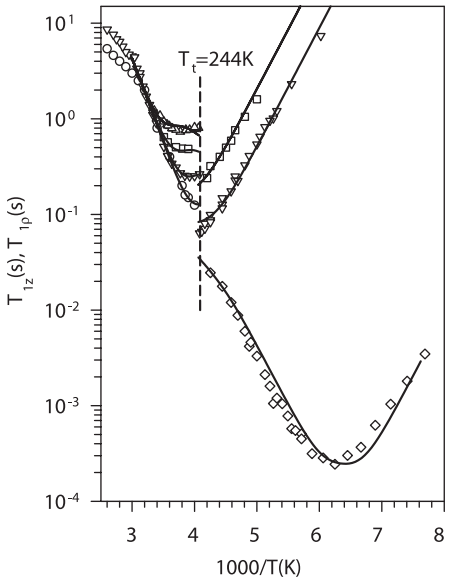

Fig. 5. Variation of ^{1}H NMR relaxation times versus $10^3/T$(K): T_{1z}: (◯) 48 MHz, (▽) 100 MHz), (□) 200 MHz), (△) 400 MHz; $T_{1\rho}$ (◊). The continuous curves correspond to a Frenkel model refinement (Eqs. (4, 5)).

The experimental data were calculated with the relation:

$$\frac{1}{T_{1z}} = \frac{1}{T_{1z}^{Rot}} + \frac{1}{T_{1z}^{SD}}. \qquad (17)$$

Using equation (17), we have calculated T_{1z} with the BPP parameters (Eq. (1); Table 2). Clearly the introduction of the Self Diffusion mechanism, represented as a solid line in Figure 2, failed to reproduce T_{1z} above T_x. This result is consistent with the relaxation dispersion curves. At $T = 301$ K and 250 K, the data are well described by the parameters of Table 2 (solid lines; Fig. 3). At higher temperatures and above $\nu_0 = 5$ MHz, the rotational contribution is too important (solid lines; Fig. 3) confirming the occurrence of a dynamical change. From the best results (Eqs. (16,17)) represented as dashed lines in Figure 3, we have obtained: $\tau_{SD} = 5.6 \times 10^{-4}$ s and 1.7×10^{-4} s at $T = 333$ K and 353 K respectively.

3.1.2 Ordered phase

In the low temperature phase, the molecular motions are investigated by proton T_2, T_{1z} (100, 200 MHz) and $T_{1\rho}$ measurements ($B_1 = 18$ G). At T_t, the freezing of the dipolar axis motion results in an large decrease of T_2 and T_{1z}. As seen in Figure 2, the phase transition prevents the

T_{1z} minimum of phase (II) to be observed. In the ordered phase, T_2 is approximatively constant above $T = 140$ K, with a limiting value consistent with the relation [22]:

$$T_2 = \frac{1}{(\gamma_H^2 M_{2R})} = 8.36 \times 10^{-6}\text{s}. \qquad (18)$$

The long correlation time approximation is valid since the T_{1z} data are proportional to B_0^2. A $T_{1\rho}$ inimum is observed at $T \approx 158$ K ($T_{1\rho} 2.4 \times 10^{-4}$s) and the relaxation curve displays the classical V-shape temperature dependence predicted by the BPP theory ($E_a = 2800$ K). An attempt to match the experimental data using equation (1) is represented in Figure 2 (Table 2, τ_{BPP}). As seen in this figure, this model is well adapted for T_{1z}, but $T_{1\rho}$ is not perfectly reproduced. The experimental data were then fitted by using equation (4), considering a 3-fold uniaxial rotation (τ_{m3}) and assuming that the φ_i terms remain equal to their values of Table 1. As seen in Figure 5, a good description is obtained with the parameters of Table 2.

In phase II, the calculated second moment are given as a solid line in Figure 1, using the approximate expression [22,31,32]:

$$M_2^{\text{exp}} = \overline{M_2} + (M_{2R} - \overline{M_2})\frac{2}{\pi}\tan^{-1}(\gamma_H^2 M_2^{\frac{1}{2}}\tau). \qquad (19)$$

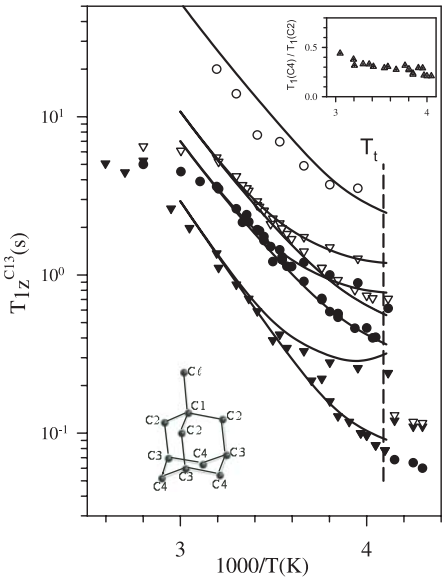

Fig. 6. NMR ^{13}C relaxation data at 25 and 100 MHz: (◯) C_1, (●) C_2, (▽) C_3, (▼) C_4. The continuous curves correspond to the refinement carried out using a Frenkel model (Eq. (6)). Inset: ratio T_1(C4)/T_1(C2) versus 1000/T(K). Indexation of the different carbons of a CL-ADM molecule is displayed on the figure. Below $T_t = 250$ K, (phase II), several temperatures were investigated at 25 MHz.

4 Analysis of ^{13}C data

The ^{13}C experimental results (25 and 100 MHz) are represented in Figure 6 for: C_1(C-Cl), C_2(CH_2), C_3(CH) and C_4(CH_2), referred according to their distances to the chlorine atom (see inset of Fig. 6). As for ^{1}H experiments, a change of E_a is observed around T_x. Below T_x we have obtained: $E^{C1} \approx 2400$ K, $E^{C2} \approx E^{C3} \approx 2900$ K, $E^{C4} \approx 3250$ K. Under the hypothesis of an isotropic model, we should observe: $T_{1z}^{C_2} \approx 0.63\ T_{1z}^{C_3} \approx T_{1z}^{C_4}$, whereas at $T = 300$ K the experimental T_{1z}^{C} are related together by the relation: $T_{1z}^{C_2} \approx 0.58\ T_{1z}^{C_3} \approx 3.06\ T_{1z}^{C_4}$. From these considerations, a BPP model is unable to describe the ^{13}C relaxation rates. With a Frenkel model we have obtained a good description of the experimental data with the parameters given in Table 2 (Fig. 6). In Figure 7, we have represented at $T = 250$ K the calculated Ψ_α (Eqs. (5, 6)). The main contribution arises from the term Ψ_4 ($\approx \Psi_{total}$). As Ψ_4 depends linearly of τ_{c3} (Tab. 1), the dipolar axis motion gives the main contribution to the relaxation both in ^{13}C and ^{1}H. However for C_2 and C_3, a second contribution arises from the term Ψ_2 which introduces the uniaxial rotation. This explains the differences between the activation energies measured directly from the slope of the relaxation curves.

In the frame of a Frenkel model, the T_{1z}^{C} ratio can be calculated from Equation (6). By assuming $\alpha = 2$, 4, we have obtained: $T_{1z}^{C_2} \approx 0.57\ T_{1z}^{C_3} \approx 2.95\ T_{1z}^{C_4}$. Below T_x, this relation is fully consistent with the experimental data. Upon increasing the temperature this ratio increases, reflecting a progressive evolution from an anisotropic behaviour to a quasi free isotropic process (inset of Fig. 6).

In phase II, only several temperatures were investigated at 25 MHz (Fig. 6). The phase transition results in an important decrease of T_{1z}^{C}, with: $T_{1z}^{C_4} \approx T_{1z}^{C_3} \approx 1.9\ T_{1z}^{C_2}$. From equation (10) we have obtained the following relations which are fully consistent with the experimental data:

$$\frac{T_{1z}^{C_4}}{T_{1z}^{C_3}} \approx 0.8; \quad \frac{T_{1z}^{C_4}}{T_{1z}^{C_2}} \approx 1.9; \quad \frac{T_{1z}^{C_3}}{T_{1z}^{C_2}} \approx 1.6. \qquad (20)$$

Consequently, another interesting feature of the Frenkel model concerns the possibility to account for the dynamical changes observed at the ordered-disordered phase transition.

5 Discussion

Frequency dependent NMR measurements is a powerful tool for molecular dynamics investigation. However, the task of finding a motional model for the description of NMR relaxation times variations is not easy. Usually a BPP expression of the correlation functions is used. This model, originally developed for liquids, ignores the physical peculiarities of solids such as molecular equilibrium positions. Consequently only a mean residence time is measured and the description of multi frequencies measurements is generally impossible. Using a Frenkel model, resulting from X-ray analysis, a much better understanding of the dynamics can be achieved. Moreover this model is suitable for explaining ^{13}C relaxation rates,

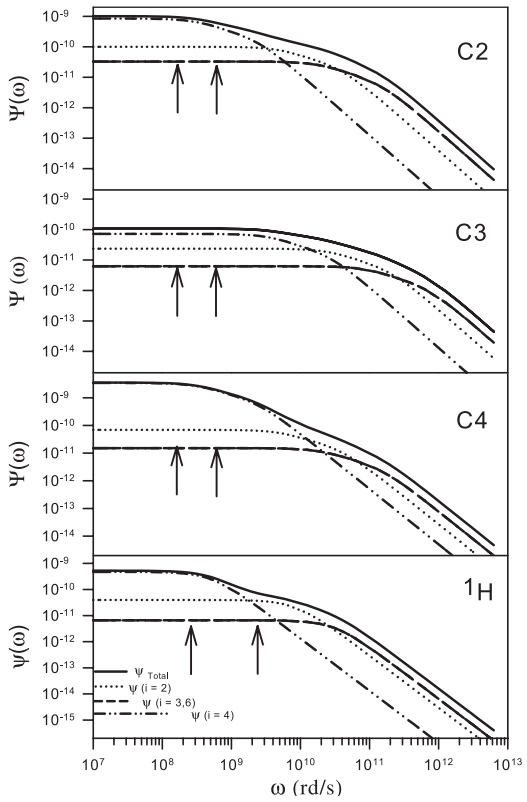

Fig. 7. Frequency dependence of $\Psi_{\iota=2;4}(\omega)$ at $T = 250$ K for protons (H) and carbons (C4, C3, C2) calculated for the rotational motions by using a Frenkel model. The full lines correspond to $\Psi_{Total}(\omega)$ and arrows delimit the frequencies domain of NMR measurements used in this work.

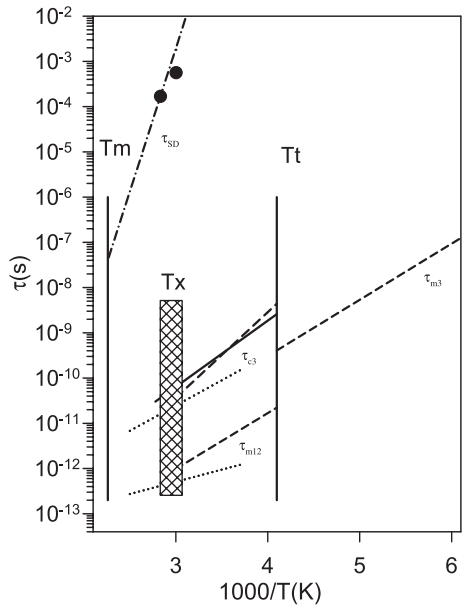

Fig. 8. Arrhenius diagram of the residence times measured on CL-ADM (Tabs. 2 and 3), by dielectric relaxation (solid line; [33]), IQNS (dotted lines; [29]), FCNMR (τ_{SD}: ●), and NMR (rotational: dashed lines; self-diffusion: dashed-dotted lines). The dynamic crossover region is delimited by a hatched zone.

which probes intramolecular interaction, above and below an ordered-disordered phase transition. In accordance with previous analysis of the PC phase, we have found that the NMR results are well fitted by assuming that the molecules exhibit a uniaxial rotation around the symmetry axis, this axis reorienting itself via 90° jumps. This latter motion is locked at the phase transition. In Figure 8, we have compared the time constants obtained by NMR to other methods: neutron scattering (IQNS; [15,29]) and dielectric relaxation [33]. All together, a good agreement is observed between these different technics, and the temperature dependence of the residence times is found Arrhenius like. However, contrary to our results, IQNS predicts a T_{1z} minimum connected to the uniaxial rotation below $T = 125$ K. This discrepancy can be explained by the deconvolution procedure used in IQNS [29]. At T_t the dipolar axis motion is still fast: $\tau_{c3} = 4 \times 10^{-9}$ s. This very fast dynamic explains the impossibility for CL-ADM to reach a glassy state. Below T_x, the residence times (τ_{c3}, τ_{m12}) are well separated in time and we found $E_a(\tau_c)/E_a(\tau_m) = 1.5$ instead of 4.6 for CN-ADM. However the global motion of CL-ADM cannot be considered as isotropic below T_x (inset of Fig. 6). The plastic phase of CL-ADM exhibits a dynamic disorder intermediate between CN-ADM where the motions are decoupled and fluoroadamantane (or ADM) where the motions are quasi-isotropic [9,19]. These behaviors are correlated to steric hindrance resulting in different form of cooperativity which are the fundamental aspect of molecular reorientations in PC. A confrontation of different plastic crystals, analysed with the BPP models, shows that $\tau(T_m) \approx 10^{-12}$ s [2]. 1-adamantanes derivatives generally conform to this trend. As seen in Figure 8, for CL-ADM this value is reached close to the temperature T_x, where MD simulations predicted a change in the rotational dynamics [9]. This dynamical change, in the pico-nanosecond regime, has already been observed by Raman [34] and neutron spin-echo experiments [15]. An anomaly in the heat capacity observed in this temperature range support this hypothesis [35]. From T_{1D} ($T_{1\rho}$) and FCNMR measurements, we have characterized the self diffusion mechanism and we have shown that SD influence T_{1z} around $T \approx 400$ K i.e 50 K above T_x. Thus this mechanism has to be discarded from the origin of the breakdown observed. This leads us to distinguish two distinct dynamical domains: below T_x where the NMR data are well described by a Frenkel model, and above T_x where this model becomes inadapted. As a consequence we expect that some hypothesis of the Frenkel model, in particular the finite number of equilibrium positions, becomes irrelevant at high temperature. Upon decreasing the temperature the dynamic turns from a liquid-like dynamics to a jumplike motion between preferential orientations.

These results call for new investigations of plastic crystals in order to confirm the existence of two distinct dynamical regimes i.e an evolution from a quasi-free rotational diffusion to activated gear tumblings motion at some critical temperature T_x.

6 Conclusion

We have presented an analysis of the dynamical properties of the molecular crystal 1-chloroadamantane using ^{13}C and ^{1}H NMR relaxation times measurements. By conventional and field-cycling NMR we have covered a broad Larmor frequencies domain ranging from 0.1 MHz to 400 MHz. In order to disentangle the different dynamical contributions to the NMR relaxation pattern, we have calculated the spectral densities adapted to the molecular symmetry of CL-ADM (Frenkel model). This model is useful, particularly for rigid molecules such as plastic crystals for which a precise knowledge of the structural properties is possible. Using this model, the dynamic disorder of CL-ADM has been characterized over a wide temperature range. While rotational motions controlled the relaxation rates at lower temperatures, we have shown that an additional self-diffusion mechanism plays an important role close to T_m. The characteristic times of this slow motion have been determined by a combination of dipolar relaxation (T_{1D}) and field-cycling measurements. However this latter mechanism is unable to describe the modifications observed in the temperature dependence of T_{1z} above the crossover temperature predicted by MD simulations. These results confirm the change from a quasi-free molecular rotation to a discrete jumps regime at T_x.

The authors thank Dr J. Virlet for providing the NMR measurements at 48 MHz and for the jump model description. The collaboration with Stelar srl (Italy) for FCNMR experiments is also acknowledged.

References

1. J. Timmermans, J. Chim. Phys. **35**, 331 (1938)
2. J.N. Sherwood, *The plastically Crystalline State* (Wiley, New York, 1979)
3. R. Bohmer, G. Diezemann, G. Hinze, E. Rössler, Prog. Nucl. Magn. Reson. Spectrosc. **39**, 191 (2001)
4. R. Brand, P. Lunkenheimer, A. Loidl, J. Chem. Phys. **116**, 10386 (2002)
5. J.P. Amoureux, R. Decressain, M. Sahour, E. Cochon, J. Phys. II France **2**, 249 (1992)
6. F. Affouard, J.F. Willart, M. Descamps, J. Non Cryst. Solids **9**, 307 (2002)
7. S.A. Lusceac, I. Roggatz, P. Medick, J. Gmeiner, E. Rössler, J. Chem. Phys. **121**, 4770 (2004)
8. S.A. Lusceac, I. Roggatz, J. Gmeiner, E. Rössler, J. Chem. Phys. **126**, 14701 (2007)
9. F. Affouard, E. Cochin, R. Decressain, M. Descamps, Europhys. Lett. **53**, 611 (2001)
10. A. Fuchs, J. Virlet, D. Andre, H.J. Szwarc, J. Chim. Phys. **82**, 293 (1985)
11. J.P. Amoureux, M. Bee, J.L. Sauvajol, Mol. Phys. **45**, 709 (1982)
12. M. Foulon, T. Belgrand, C. Gors, M. More, Acta Crystallogr. B **45**, 404 (1989)
13. T. Clark, T.Mc.O. Knox, H. Mackle, M.A.Mc Kervey, J.C.S. Faraday I **73**, 1224 (1977)
14. W. Gotze, L. Sjogen, Rep. Prog. Phys. **55**, 241 (1992)
15. F. Affouard, E. Cochin, R. Decressain, M. Descamps, W. Haeussler, Physica B **350**, E1087 (2004)
16. R. Kimmich, *NMR tomography, diffusometry, Relaxometry* (Springer, Berlin, 1997)
17. L. Quiroga, thesis, Université Paris VI (1982)
18. S. McGuigan, J.M. Chezeau, M. Nasser, J. Phys. **46**, 271 (1985)
19. R. Decressain, J.P. Amoureux, L. Carpentier, J.B. Nagy, Mol. Phys. **73**, 553 (1991)
20. R. Decressain, J.P. Amoureux, E. Cochon, Phys. Stat. Sol. (b) **190**, 295 (1995)
21. J. Jeener, P. Broekaert, Phys. Rev. **157**, 232 (1967)
22. A. Abragam, *The principles of Nuclear Magnetism* (Clarendon Press, Oxford, 1961)
23. *Encyclopedia of Nuclear Magnetic Resonance* (John Wiley and sons, New York, 1996)
24. N. Bloembergen, E.M. Purcell, R.V. Pound, Phys. Rev. **73**, 679 (1948)
25. C.J. Bradley, A.P. Cracknell, *The Mathematical Theory of Symmetry in Solids* (Clarendon Press, Oxford, 1972)
26. J. Virlet, L. Quiroga, B. Boucher, J.P. Amoureux, M. Castelain, Mol. Phys. **48**, 1289 (1983)
27. A. Guillermo, R. Dupeyre, J.P. Cohen-Addad, Macromolecules **23**, 1291 (1990)
28. N.E. Moe, H.Q. Xiao, M.D. Ediger, Macromolecules **33**, 2145 (2000)
29. M. Bee, J.P. Amoureux, Mol. Phys. **48**, 63 (1983)
30. A.H. Resing, Mol. Cryst. **9**, 101 (1969)
31. H.S. Gutowsky, G. Pake, J. Chem. Phys. **18**, 162 (1950)
32. E.R. Andrew, J. Lipofski, J. Magn. Res. **8**, 217 (1972)
33. J.P. Amoureux, M. Sahour, C. Fernandez, P. Bodart, Phys. Stat. Sol. (a) **143**, 441 (1994)
34. F. Affouard, A. Hedoux, Y. Guinet, T. Denicourt, M. Descamps, J. Phys: Condens. Matter **13**, 7237 (2001)
35. K. Kobashi, T. Kyomen, M. Ogumi, J. Phys. Chem. Solids **59**, 667 (1988)